Elastic Model of Deformable Fingertip for Soft-fingered Manipulation

Takahiro Inoue, *Student Member, IEEE,* and Shinichi Hirai, *Member, IEEE*

***Abstract*— We propose straightforward static elastic model of a hemispherical soft fingertip undergoing large contact deformation, as occurs when robotic hands with the fingertips handle and manipulate objects, which is suitable for the analysis of soft-fingered manipulation because of the simple form of the model. We focus on formulating elastic force and potential energy equations for the deformation of the fingers which are represented as an infinite number of virtual springs standing vertically. The equations are functions of two variables: the maximum displacement of the hemispherical fingertip and the orientation angle of a contacting planar object. The elastic potential energy has a local minimum (LMEE) in our model. The elastic model was validated by comparison with results of a compression test of the hemispherical soft fingertip.**

***Index Terms*— Soft fingertip, Manipulation, Grasping, Robotic hand, Elasticity, Deformation model.**

I. Introduction

To date, various research has been done on manipulations of objects by soft-fingered robotic hands. Most of the studies, particularly earlier studies, focused only on contact mechanisms on various soft fingers. More recently, there has been an increase in studies on sensing mechanisms of human hand and designing control systems in robotic applications to emulate the human capabilities which are applicable to robotic hands. The conventional studies, however, have not been explicitly providing any analytical exploration of the simplicity in grasping and manipulating motions in terms of the soft-fingered handling. As a cause of the above mention, it has been substantially difficult to derive a fine elastic model of soft materials used in the fingertips.

Yokokohji *et al.* proposed a control scheme with visual sensors which can cancel the frictional twist/spin moment at the contact point of soft fingertips, and achieved stable grasping by spherical soft fingertips [1], [2]. Maekawa *et al.* developed a finger-shaped tactile sensor covered with a soft and thin material, and proposed a control algorithm based on tactile feedback using the sensor, which needs no information about the geometry of the grasped object [3], [4]. They managed to control the position of an object along a desired trajectory. In these papers, point-contacts were used to represent constraints of rolling contact in their theoretical models, although the fingertips were made from soft material such as rubber. Arimoto *et al.* verified the passivity of equations of motion for a total handling system by using a Lagrangian function incorporating the elastic potential energy due to the deformation of soft fingertips [5], and compensated for the gravity effect in three-dimensional space [6]. An elastic force model was also derived for the elastic potential energy of a system in which virtual linear springs were arranged for simplicity in a radial pattern inside hemispherical soft fingertips. Doulgeri *et al.* discussed the problem of stable grasping with deformable fingertips on which rolling constraints were described as non-holonomic because of change in the effective rolling radius of the soft fingertip [7], [8]. The above studies, however, focused mainly on deriving a control law to realize stable grasping and pose control of the grasped object, not on revealing a physically appropriate deformation model, which also contains the nonlinear characteristics of a hemispherical soft fingertip.

On the other hand, Xydas *et al.* proposed an exact deformation model based on the mechanics of the materials containing nonlinear characteristics, and performed Finite Element (FE) analysis for a hemispherical soft fingertip [9], [10]. Kao *et al.* experimentally demonstrated that the elastic force due to deformation satisfied a power law with respect to the displacement of the fingertip, and insisted that their theory subsumes Hertzian contact [11]. These studies, however, did not distinguish between the material nonlinearity of the soft fingertip and the geometrical nonlinearity caused by the hemispherical shape of the fingertip, and defined a parameter including the effect of both nonlinearities. Consequently, the cause of the discrepancy between the results of the simulation based on their model and the results of actual experiments was not apparent. In addition, because of the complexity of their proposed models, these studies do not lend themselves to analysis of equations of motion for the soft-fingered manipulation system overall. While FE analysis may enable us to derive a stress distribution and an elastic force on the soft fingertip, these simulation results depend on the selected mesh pattern. Although FE analysis based on a certain arbitrary mesh pattern may prove the stability for equations of motion of the handling system, it does not always provide proof of stability for equations derived from other mesh patterns.

In this report, we propose a static elastic model of a hemispherical soft fingertip in a physically reasonable and straightforward form suitable for theoretical analysis of robotic handling motions. We distinguish between geometric nonlinearity due to the hemispherical shape and material nonlinearity of soft materials, i.e., the nonlinearity of the Young's modulus of the soft material, allowing us to focus only on the geometric nonlinearity of the soft fingertip, and analytically formulate elastic force and elastic potential energy equations for the deformation of the fingertip. We show that each equation is a function of two variables: the maximum displacement of the

Manuscript received October 6, 2005; revised October 6, 2005. This work was supported by the IEEE.

The authors are with the Laboratory for Integrated Machine Intelligence, Department of Robotics, Ritsumeikan University, Japan (e-mail: gr018026@se.ritsumei.ac.jp;hirai@se.ritsumei.ac.jp).

fingertip and the orientation angle of a contacting object. We also show that when the object is positioned normal to the fingertips, the elastic potential energy is minimum. We finally validate the static elastic model by conducting a compression test of the hemispherical soft fingertip and comparing the results.

II. Static Elastic Model of Hemispherical Soft Fingertip

We treat the fingertips as if they were composed of an infinite number of virtual linear springs standing vertically. Fig.1 shows one such spring. We formulate elastic force and elastic potential energy equations for the deformation of the fingertip. In order to simplify the derivation process of both equations, two assumptions associated with material characteristics are given as follows:

1) The incompressibility of elastomer materials is not dealt with.
2) Young's modulus is constant.

Note that the contact condition being discussed in the present study is restricted to the case that an applied force to the fingertip is assumed to be along z-axis of the fingertip. In addition, we consider that an object never comes into contact with the underneath plane of the fingertip.

A. Fingertip Stiffness

Let us apply an infinitesimal virtual spring QR with sectional area dS inside the soft fingertip, as shown in Fig.1. Let dF be the infinitesimal elastic force due to the shrinkage PQ of the virtual spring. Let θ_p be the orientation angle of the contacting object, a be the fingertip radius, d be the maximum displacement of the fingertip, $a_c = \sqrt{a^2-(a-d)^2}$ be the radius of the contacting circle, and P be the point where the spring is in contact with the object. Furthermore, let θ be the angle subtended between line PQ and the z-axis, and ϕ be the azimuthal angle on the xy-plane. Using the contact surface equation, $x\sin\theta_p + z\cos\theta_p = a-d$ (see Appendix I), the infinitesimal elastic force dF is given by

$$\mathrm{d}F = k\cdot PQ = k\left\{\sqrt{a^2-(x^2+y^2)} - \frac{a-d-x\cdot\sin\theta_p}{\cos\theta_p}\right\}, \quad (1)$$

where k is the spring constant of the spring QR. Note that k is proportional to the sectional area dS and inversely proportional to the natural length $\sqrt{a^2-(x^2+y^2)}$. Letting E be the Young's modulus of soft finger materials, k is described as (see Appendix II)

$$k = \frac{E\ \mathrm{d}S}{\sqrt{a^2-(x^2+y^2)}}. \quad (2)$$

Letting K be the fingertip stiffness on the entire deformed part illustrated in Fig.1, K can be expressed from Eq. (2) as

$$K = \iint_{ell} k = E\int_{-a_c}^{a_c}\int_{b_1(y)}^{b_2(y)} \frac{\mathrm{d}x\,\mathrm{d}y}{\sqrt{a^2-(x^2+y^2)}}, \quad (3)$$

where

$$b_1(y) = (a-d)\sin\theta_p - \cos\theta_p\sqrt{a_c^2-y^2}, \quad (4)$$

$$b_2(y) = (a-d)\sin\theta_p + \cos\theta_p\sqrt{a_c^2-y^2}, \quad (5)$$

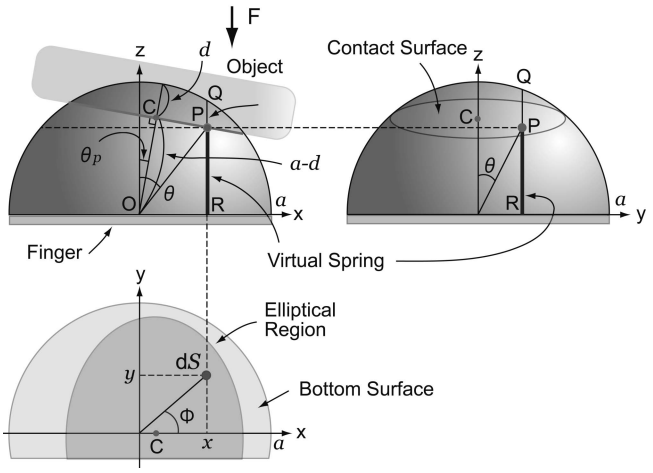

Fig. 1. Contact mechanism

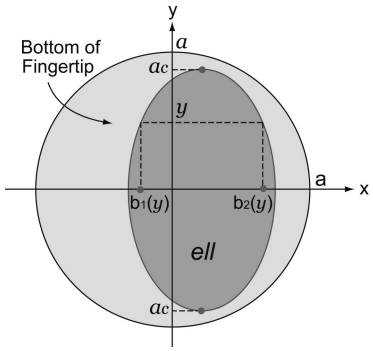

Fig. 2. Integration area.

and *ell* denotes the elliptical region shown in Fig.2-(a). Applying a numerical integration to Eq. (3), we obtain a constant fingertip stiffness depicted as continuous lines, as shown in Fig.3. This indicates that the fingertip stiffness K is independent of the object orientation θ_p. Hence, in this study we additionally provide the thir assumption that:

3) the fingertip stiffness is independent of the object orientation as long as the maximum displacement remains constant.

By using the above assumption, we formulate the fingertip stiffness K in an analytical formula.

Now, performing a substitution that $x = r\cos\phi\cos\theta_p + (a-d)\sin\theta_p$ and $y = r\sin\phi$, Eq. (3) is then transformed into (see Appendix III)

$$K = E\int_0^{a_c} r\left\{\int_0^{2\pi} \frac{\cos\theta_p\ \mathrm{d}\phi}{\sqrt{a^2-\{x^2(r,\phi)+y^2(r,\phi)\}}}\right\}\mathrm{d}r. \quad (6)$$

Since assumption 3) claims K is independent of θ_p, we can substitute $\theta_p = 0$ into Eq. (6), and get

$$K = E\int_0^{a_c} r\left\{\int_0^{2\pi} \frac{\mathrm{d}\phi}{\sqrt{a^2-r^2}}\right\}\mathrm{d}r = 2\pi E d. \quad (7)$$

Plotting the simulation result of Eq. (7) as dotted lines onto Fig.3 together with the results of Eq. (3), we find that both

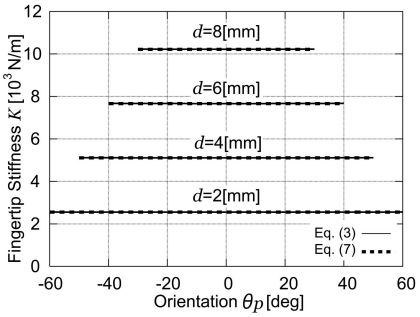

Fig. 3. Comparison between numerical results of Eq. (3) and analytical simulations of Eq. (7) when $E = 0.2032$ MPa measured in the present study.

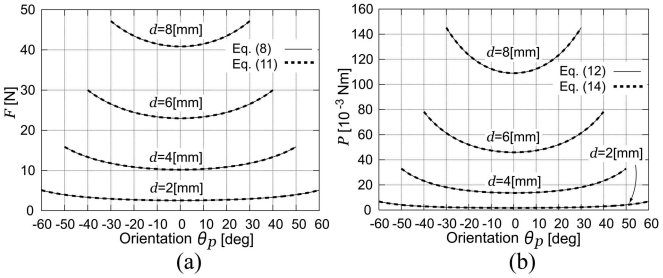

Fig. 4. Comparison between the numerical integration and the analytical simulation of F and P, respectively: (a) elastic force, (b) elastic energy.

lines coincide with each other. This implies that the third assumption due to the numerical observation is appropriate, and additionally the stiffness is a function of only the maximum displacement d.

B. Elastic Force

Likewise, by using the third assumption associated with the fingertip stiffness, we formulate the elastic force and potential energy equations in a straightforward way. Using Eqs. (1), (2) and a geometrical relationship $QT = PQ\cos\theta_p$ (see Fig.14 in Appendix III), the elastic force F can be written as

$$\begin{aligned} F &= \frac{1}{\cos\theta_p}\int\!\!\int_{ell} k\cdot QT \\ &= \frac{E}{\cos\theta_p}\int_{-a_c}^{a_c}\int_{b_1(y)}^{b_2(y)} \frac{QT\cdot \mathrm{d}x\,\mathrm{d}y}{\sqrt{a^2-(x^2+y^2)}}. \end{aligned} \tag{8}$$

Performing the same variable conversion as the derivation process of K, Eq. (8) is then transformed as

$$F = \frac{E}{\cos\theta_p}\int_0^{a_c} QT(r)\cdot r\left\{\int_0^{2\pi} B(r,\phi)\ \mathrm{d}\phi\right\}\mathrm{d}r, \tag{9}$$

where (see Fig.14)

$$QT(r) = \sqrt{a^2-r^2} - (a-d). \tag{10}$$

In Eq. (9), $B(r,\phi)$ corresponds to the integrand within the braces in Eq. (6). Here applying the assumption 3) to $B(r,\phi)$ as well as Eq. (7), F is finally calculated as

$$F = \frac{E}{\cos\theta_p}\int_0^{a_c} QT(r)\cdot r\left\{\int_0^{2\pi}\frac{\mathrm{d}\phi}{\sqrt{a^2-r^2}}\right\}\mathrm{d}r = \frac{\pi E d^2}{\cos\theta_p}. \tag{11}$$

C. Elastic Potential Energy

As well as Eq. (8), the elastic potential energy P is expressed as

$$\begin{aligned} P &= \frac{1}{2}\int\!\!\int_{ell} k\cdot PQ^2 = \frac{1}{2\cos^2\theta_p}\int\!\!\int_{ell} k\cdot QT^2 \\ &= \frac{E}{2\cos^2\theta_p}\int_{-a_c}^{a_c}\int_{b_1(y)}^{b_2(y)} \frac{QT^2\cdot \mathrm{d}x\,\mathrm{d}y}{\sqrt{a^2-(x^2+y^2)}}. \end{aligned} \tag{12}$$

Performing the same variable conversion as the derivation process of F, Eq. (12) is then transformed as

$$P = \frac{E}{2\cos^2\theta_p}\int_0^{a_c} QT^2(r)\cdot r\left\{\int_0^{2\pi} B(r,\phi)\ \mathrm{d}\phi\right\}\mathrm{d}r. \tag{13}$$

Here again, applying the assumption 3) to $B(r,\phi)$ in Eq. (13), P is finally be calculated as

$$\begin{aligned} P &= \frac{E}{2\cos^2\theta_p}\int_0^{a_c} QT^2(r)\cdot r\left\{\int_0^{2\pi}\frac{\mathrm{d}\phi}{\sqrt{a^2-r^2}}\right\}\mathrm{d}r \\ &= \frac{\pi E d^3}{3\cos^2\theta_p}. \end{aligned} \tag{14}$$

Note that Eqs. (11) and (14) clarify that the elastic force and elastic potential energy on the entire deformed part of a hemispherical soft fingertip are functions of two variables, namely, the maximum displacement d and the object orientation angle θ_p. Furthermore, we find that both formulae have a local minimum when the orientation angle is zero. Especially, we describe the minimum value of elastic energy as *Local Minimum of Elastic Potential Energy*, which is abbreviated as *LMEE*.

Finally, in order to confirm the transformations of formulae from Eq. (8) to Eq. (11) and Eq. (12) to Eq. (14), we verify the numerical analysis of Eqs. (8) and (12) and simulation results of Eqs. (11) and (14). Fig.4 indicates the result, and concludes that both Eqs. (11) and (14) are mathematically reasonable formulae in the present study.

D. Relationship between Elastic Force and Elastic Energy

While the individual virtual spring used in our study is based on a linear elasticity, the entire fingertip model that is obtained by completing the double integration on an elliptical region exhibits a geometrical nonlinearity caused by the hemispherical shape of the fingertip. In other words, the completed fingertip model has a nonlinear fingertip stiffness expressed as Eq. (7). Hence, when we compute the total force Eq. (11) from the energy Eq. (14), we must define an *equivalent displacement* and use it for the differentiatial calculation.

In the case of normal contact that corresponds to $\theta_p = 0$, elastic models are given as follows:

$$P = \frac{\pi E d^3}{3}, \tag{15}$$

$$\frac{\partial P}{\partial d} = \pi E d^2 = F, \tag{16}$$

$$\frac{\partial^2 P}{\partial d^2} = 2\pi E d = K, \tag{17}$$

where d itself corresponds to the equivalent displacement.

Continuously, let us consider the case of diagonal contact when $\theta_p \neq 0$. We define Δz_{eq} as an equivalent displacement, and it must satisfy

$$\frac{\partial P}{\partial \Delta z_{eq}} = \frac{\pi E d^2}{\cos\theta_p} = F, \tag{18}$$

$$\frac{\partial^2 P}{\partial \Delta z_{eq}^2} = 2\pi E d = K. \tag{19}$$

The displacement Δz_{eq} to fulfill Eqs. (18) and (19) can be found such that a geometrical relationship $d = \Delta z_{eq}\cos\theta_p$ is maintained as shown in Fig. 14. It is obvious that Δz_{eq} means a true maximum displacement among all the virtual springs in any case that includes $\theta_p = 0$ and $\theta_p \neq 0$.

III. Comparison with Hertzian Contact

In 1881, Hertz proposed a contact theory for two elastic objects having arbitrary curved surfaces [12]. He showed that a normal contact force generated between an elastic sphere and a plane whose Young's modulus is infinity can be expressed as

$$F = \frac{4\sqrt{R}}{3}\left(\frac{E}{1-\sigma^2}\right) d^{\frac{3}{2}}, \tag{20}$$

where R is the radius, E the Young's modulus of the object, σ the Poisson's ratio, and d the maximum displacement of the sphere. Since the above equation is useful from a practical viewpoint, it has been widely used for computing the contact stress between, for example, a wheel and a rail, a roll and material, and a retainer and a ball in a bearing. However, in Hertzian contact, it is assumed that both elastic objects are open elliptic paraboloids with an arbitrary radius of curvature. Consequently, no boundary conditions are used in the Hertzian contact model.

Kao *et al.* defined the parameter c_d corresponding to a material and geometric nonlinearity [11], and transformed Eq.(20) into

$$F = c_d d^{\zeta}. \tag{21}$$

They conducted a vertical compression test using a hemispherical soft fingertip, and estimated the parameter c_d empirically by using a weighted least-squares method. It has been shown that ζ is approximately 2.3 or 1.75 when the rate of deformation of the finger is above or below 20%, respectively. In other words, the parameter ζ is not identical to 3/2 in the contact model of soft fingertips. Thus the Hertzian contact theory cannot be adopted for deriving the elastic model of the hemispherical soft fingertip.

Fig.5 shows a comparison result in which the elastic force value with respect to the displacement d is plotted when a hemispherical soft fingertip is compressed vertically, whose radius is 20 mm. It is obvious that our vertically-oriented spring model is more suitable for deriving an elastic force up to the midrange displacement of the fingertip. It is because that our model contains the geometric nonlinearity due to the hemispherical shape of the fingertip, that is, the present model could indicate that ζ becomes 2 by only adopting appropriate natural length to the individual springs.

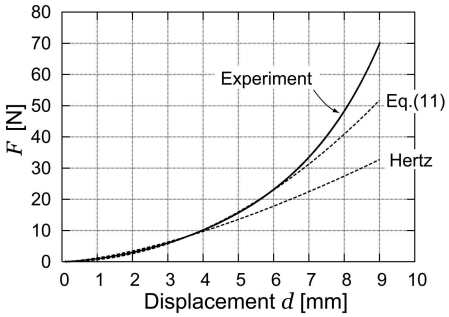

Fig. 5. Comparison between the Hertzian contact model and the present elastic force model when $\theta_p = 0$ and $E = 0.2032$ [MPa].

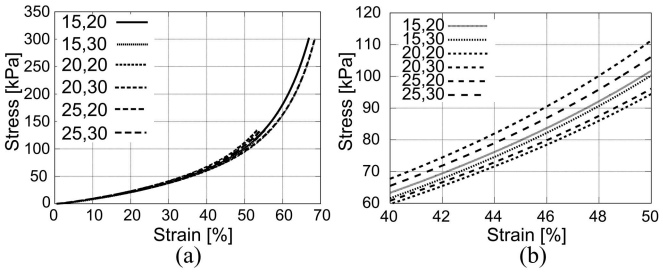

Fig. 6. Stress-strain diagram of polyurethane rubber: (a) stress-strain diagram, (b) enlarged diagram.

Soft materials exhibit nonlinear characteristics, even for infinitesimal deformations. In fact, Tatara newly derived a nonlinear Young's modulus with respect to compressive strain [13]. Furthermore, the concept for the contact angle of the object is not incorporated in the Hertzian contact theory. While the Hertzian contact theory can be utilized for a simple contact pattern corresponding to the normal contact, no contact at any other arbitrary angle or rolling contact can be defined. On the other hand the elastic models proposed in this paper cover any contact angle of the object, and therefore, these models can be used to analyze grasping and manipulating motions containing varied possible contact forms by soft-fingered robotic hand.

IV. Measurement of Young's Modulus

In the present study, the Young's modulus of the soft fingertip was measured by conducting a compression test on 6 cylinders of polyurethane gel. Three cylinders were 20 mm in diameter and 15, 20, and 25 mm in height, and three were 30 mm in diameter and also 15, 20, and 25 mm in height, as shown in Fig.8-(a).

Fig.6-(a) shows the overall view of a measured stress-strain diagram, and an enlarged view of part of the diagram is shown in Fig.6-(b). Numerical values shown in both graphs denote the specimen height on the left side and the specimen diameter on the right side. The data were averaged and smoothed using the least-squares method (LSM), as shown in Fig.7. We assumed that the maximum deformation of the soft fingertip is 50% in the radius. Furthermore, in order to focus predominantly on the geometric nonlinearity due to the hemispherical shape, we avoided the issue of the material's nonlinearity which is directly related to the Young's modulus of soft materials.

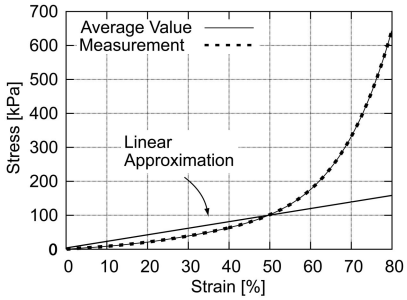

Fig. 7. Average value of stress-strain diagram.

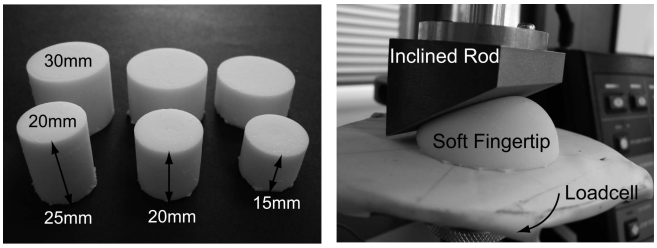

Fig. 8. Compression test of a hemispherical soft fingertip: (a) several specimens, (b) compression test.

Consequently, we performed a linear approximation for a 50% strain, as in Fig.7, and estimated the Young's modulus as 0.2032 MPa.

V. Compression Test

By compressing a hemispherical soft fingertip made of polyurethane gel along the normal direction, as shown in Fig.1 and Fig.8-(b), we verified the validity of our elastic force model represented in Eq. (11). Furthermore, by conducting multiple experiments with various contacting angles, we demonstrated the existence of the local minimum of the elastic force. In the compression test, we used a fingertip with a diameter of 40 mm, and contacting rods with thirteen different shapes. The rods were inclined from 0 to 30 deg in increments of 2.5 deg, as shown in Fig.8-(b). Fig.9 compares experiments with simulation results. The horizontal axis represents the maximum displacement of the compressed fingertip, while the vertical axis represents the elastic force measured by a loadcell placed in the compression machine.

In all the graphs in Fig.9, the simulation and experimental results are almost identical to each other up to $d = 6.0$ mm, after which the discrepancies increase with the magnitude of the displacement. The discrepancy comes from the linear approximation of the experimental stress-strain diagram shown in Fig.7. The effect leads directly to nonlinearity of Young's modulus, which is outside the scope of the present study.

Fig.10-(a) and Fig.11-(a) show simulation and experimental results, respectively. Enlarged views of both results are also shown in Fig.10-(b) and Fig.11-(b). The numerical values in each graph denote the inclined angle of the contacting object, and both results are plotted at intervals of 5.0 deg. The elastic force increases as the orientation angle increases

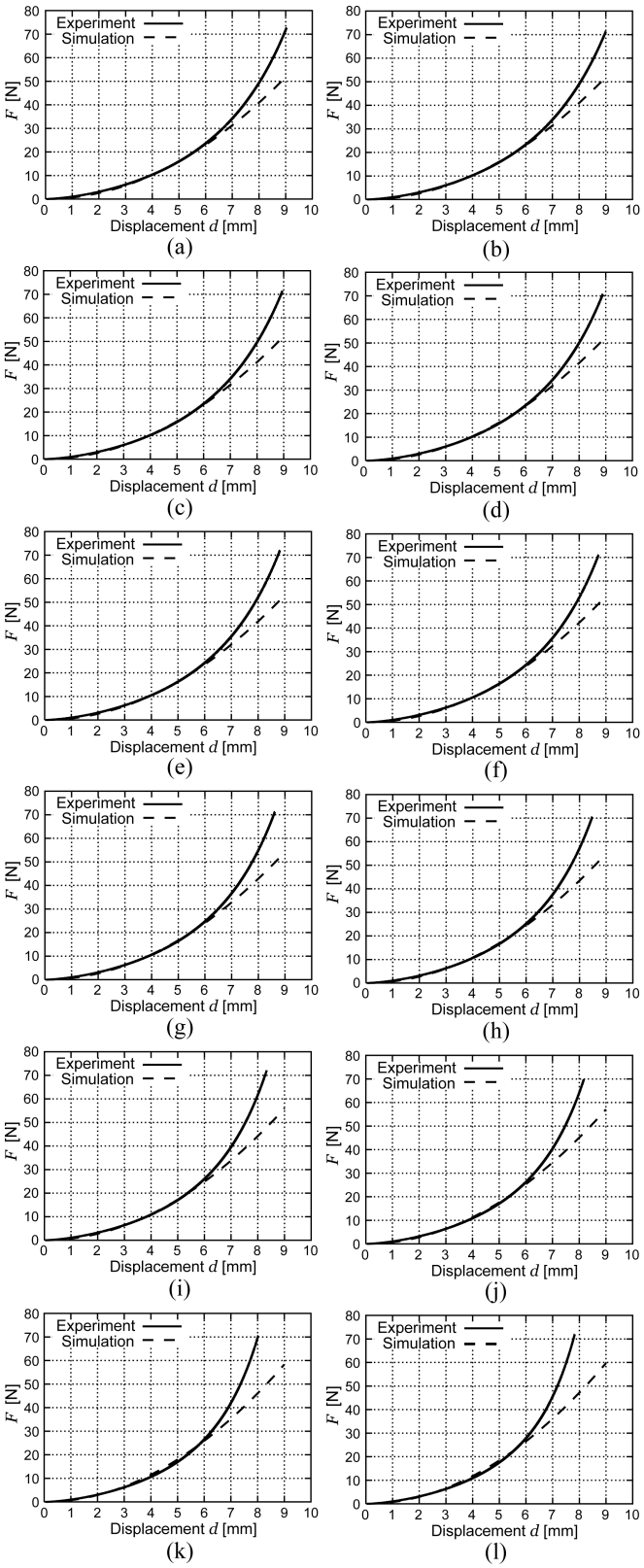

Fig. 9. Elastic forces in experiments: (a) 2.5 [deg], (b) 5.0 [deg], (c) 7.5 [deg], (d) 10.0 [deg], (e) 12.5 [deg], (f)15.0 [deg], (g) 17.5 [deg], (h) 20.0 [deg], (i) 22.5 [deg], (j) 25.0 [deg], (k) 27.5 [deg], (l) 30.0 [deg].

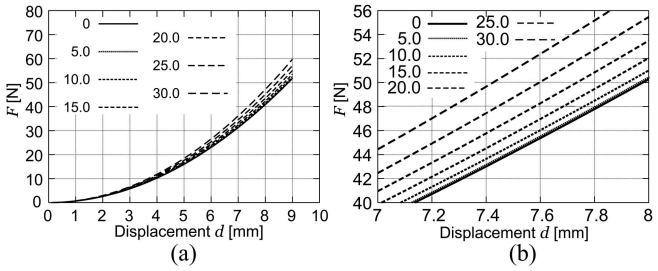

Fig. 10. Simulation results of elastic force: (a) simulations, (b) enlarged view.

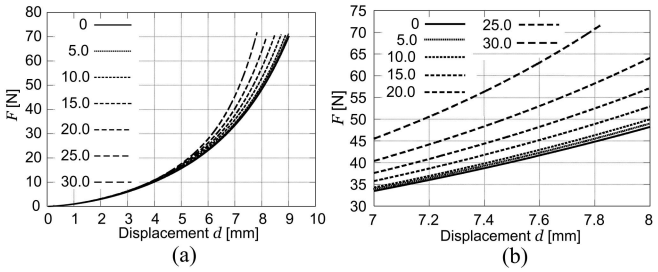

Fig. 11. Experimental results of elastic force: (a) experiments, (b) enlarged view.

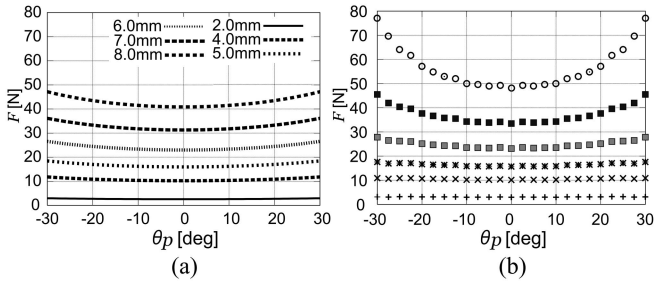

Fig. 12. Local minimum of elastic force: (a) simulations, (b) experiments.

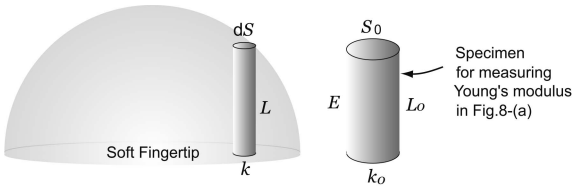

Fig. 13. Spring constant inside the soft fingertip.

under constant maximum displacement. As confirmation, we plotted the elastic force against θ_p of Eq. (11) in Fig.12. The numerical values shown in the graph denote the maximum displacement d. At about 0 deg, there is a clear local minimum of the elastic force, and the change in elastic force with θ_p is greatest when the displacement is maximum, that is, 8.0 mm. The same tendency can also be seen in the simulation results. The results therefore indicate that our proposed elastic model can present a distinctive phenomenon, i.e., a local minimum elastic force, even when the deriving process is represented simply by bringing linear virtual springs standing in the normal direction. On the other hand, the discrepancy in the large displacement shown in Fig.12 would be reduced if the Young's modulus could be defined as a nonlinear function of compression strain, and be used to adopt the model to accommodate the nonlinearity of the material. However, the present study focuses on the geometric nonlinearity, and the deriving process including both nonlinearities will be addressed in future studies.

VI. Concluding Remarks

We have formulated a static elastic force model and an elastic potential energy function based on virtual springs inside a hemispherical soft fingertip. We have also proven the existence of an LMEE and experimentally demonstrated that the elastic force due to the deformation has a local minimum. Our model requires us to only measure the Young's modulus of a corresponding material to be used in robotic fingertips. In future studies, we will consider constant volume deformation of incompressible elastomer materials, and derive elastic models incorporating a nonlinear Young's modulus.

These new findings suggest a quasi-static manipulation theory based on the LMEE for a minimum d.o.f. robotic hand [14]. By expanding the new idea of LMEE in the development of grasping and manipulation theory using soft-fingered robotic hand, it is expected that the stable grasping and the pose control of a grasped object by a minimum d.o.f. two-fingered hand may be achieved and a succinct control system will be designed.

Appendix I
Contact Plane Formula

As illustrated in Fig.1, the point C is described in a vector form as

$$\overrightarrow{OC} = \begin{bmatrix} (a-d)\sin\theta_p \\ 0 \\ (a-d)\cos\theta_p \end{bmatrix}. \tag{22}$$

In addition, a normal unit vector with respect to the contact surface is represented as

$$\mathbf{n} = \begin{bmatrix} \sin\theta_p \\ 0 \\ \cos\theta_p \end{bmatrix}. \tag{23}$$

Since the contact plane can be written by an inner product form, $\left\{ [x,y,z]^T - \overrightarrow{OC} \right\} \cdot \mathbf{n} = 0$, the plane equation is therefore described as follows:

$$x\sin\theta_p + z\cos\theta_p = a - d. \tag{24}$$

Appendix II
Spring Constant Formulation

As shown in Fig.13, letting k_0, dS_0, and L_0 respectively be the spring constant, the sectional area, and the natural length of a specimen for measuring the Young's modulus, and E be the Young's modulus obtained from an appropriate compression

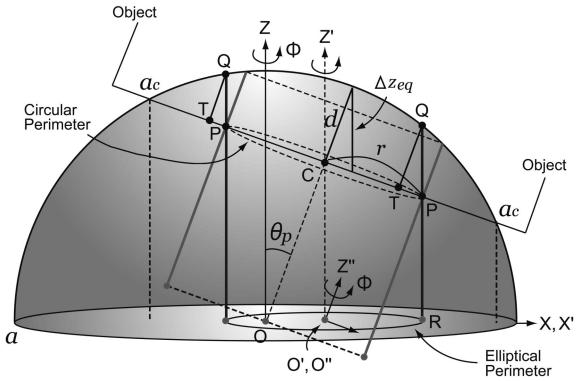

Fig. 14. Equivalent fingertip stiffness with respect to $\sum''$-coordinate system.

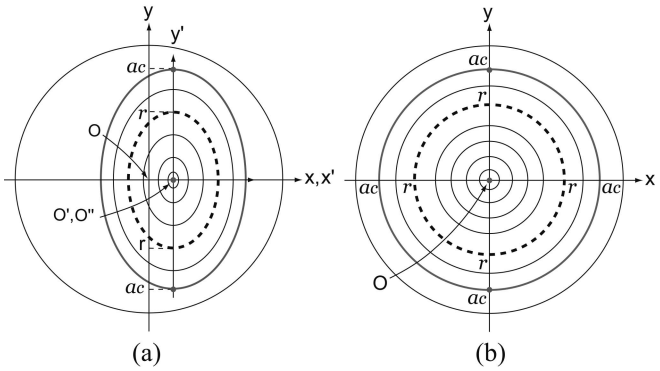

Fig. 15. Fingertip stiffness on a certain perimeter: (a) elliptical perimeter, (b) circular perimenter.

test, we can derive the following equations according to linear material mechanics:

$$\sigma = E\varepsilon \tag{25}$$

$$\Longleftrightarrow \qquad \frac{F}{S_0} = E\frac{\delta x}{L_0} \tag{26}$$

$$\Longleftrightarrow \qquad E = \frac{L_0}{\delta x}\cdot\frac{F}{S_0} = \frac{L_0}{\delta x}\cdot\frac{k_0\delta x}{S_0} = k_0\frac{L_0}{S_0}, \tag{27}$$

where F denotes an applied force to the specimen and δx is a displacement in the identification test. Since this paper assumes that the Young's modulus is an invariant physical value for individual material, the following equation is satisfied:

$$k\frac{L}{\mathrm{d}S} = k_0\frac{L_0}{S_0} = E \tag{28}$$

$$\Longleftrightarrow \qquad k = E\frac{\mathrm{d}S}{L} = \frac{E\,\mathrm{d}S}{\sqrt{a^2-(x^2+y^2)}}. \tag{29}$$

APPENDIX III
COORDINATE CONVERSION TO DERIVE THE FINGERTIP STIFFNESS

As illustrated in Fig.14, let $\sum'$ be the coordinate system translated to O' from the $\sum$ frame, and $\sum''$ be the cylindrical coordinate system inclined by θ_p from z'-axis. Let r be the arbitrary radius on the contact circle that has an origin C, and ϕ be the common rotational angle around the z-, z'-, and z''-axes. The relationship between (x',y') on the $\sum'$ frame and (r,ϕ) on the $\sum''$ frame is then expressed as

$$x' = r\cos\phi\cos\theta_p, \tag{30}$$

$$y' = r\sin\phi. \tag{31}$$

Since the relationship between (x,y) and (x',y') is described as $x = x' + (a-d)\sin\theta_p$ and $y = y'$, the variable transformation through the coordinate systems $\sum$ and $\sum''$ can be expressed as

$$x = r\cos\phi\cos\theta_p + (a-d)\sin\theta_p, \tag{32}$$

$$y = r\sin\phi. \tag{33}$$

Simultaneously, the elliptical region at the bottom surface of the fingertip shown in Fig.14 can be converted to a circular region according to the above transformation rule, that is, the integration area of (r,ϕ) varies at $[0,a_c]$ and $[0,2\pi]$, respectively.

Next, let us consider the physical meaning of the double integration of $B(r,\phi)$ used in Eqs. (9) and (13), which is detailed in Eq. (6) as:

$$\int_0^{2\pi} B(r,\phi)\ \mathrm{d}\phi = \int_0^{2\pi}\frac{\cos\theta_p\ \mathrm{d}\phi}{\sqrt{a^2-\{x^2(r,\phi)+y^2(r,\phi)\}}}. \tag{34}$$

Eq. (34) corresponds to a stiffness on an elliptical perimeter whose longitudinal radius is r, as shown in Fig.15-(a). Additionally, substituting $\theta_p = 0$ into Eq. (34) enables to obtain an equivalent stiffness on a circular perimeter of radius r shown in Fig.15-(b).

REFERENCES

[1] Y.Yokokohji, M.Sakamoto, and T.Yoshikawa, "Vision-Aided Object Manipulation by a Multifingered Hand with Soft Fingertips," in *Proc. IEEE Int. Conf. Robot. Autom.*, pp.3201-3208, 1999.

[2] Y.Yokokohji, M.Sakamoto, and T.Yoshikawa, "Object Manipulation by Soft Fingers and Vision," in *Proc. 9th Int. Symposium of Robotics Research*, pp.365-374, 2000.

[3] H.Maekawa, K.Komoriya, and K.Tanie, "Manipulation of an Unknown Object by Multifingered Hands with Rolling Contact Using Tactile Feedback," in *Proc. IEEE Int. Conf. Intell. Robots Syst.*, pp.1877-1882, 1992.

[4] H.Maekawa, K.Tanie, K.Komoriya, M.Kaneko, C.Horiguchi, and T.Sugawara, "Development of a Finger-Shaped Tactile Sensor and its Evaluation by Active Touch," in *Proc. IEEE Int. Conf. Robot. Autom.*, pp.1327-1334, 1992.

[5] S.Arimoto, P.Nguyen, H.Y.Han, and Z.Doulgeri, "Dynamics and Control of a set of Dual Fingers with Soft Tips," *Robotica*, vol.18, pp.71-80, 2000.

[6] S.Arimoto, Z.Doulgeri, P.Nguyen, and J.Fasoulas, "Stable Pinching by a pair of Robot Fingers with Soft Tips under the Effect of Gravity," *Robotica*, vol.20, pp.241-249, 2002.

[7] Z.Doulgeri, J.Fasoulas, and S.Arimoto, "Feedback Control for Object Manipulation by a pair of Soft Tip Fingers," *Robotica*, vol.20, pp.1-11, 2002.

[8] Z.Doulgeri and J.Fasoulas, "Grasping Control of Rolling Manipulation with Deformable Fingertips," *IEEE/ASME Trans. Mechatronics*, vol.8, no.2, pp.283-286, 2003.

[9] N.Xydas and I.Kao, "Modeling of Contact Mechanics and Friction Limit Surfaces for Soft Fingers in Robotics, with Experimental Results," *J. Robotics Research*, vol.18, no.8, pp.941-950, 1999.

[10] N.Xydas, M.Bhagavat, and I.Kao, "Study of Soft-Finger Contact Mechanics Using Finite Elements Analysis and Experiments," in *Proc. IEEE Int. Conf. Robot. Automat.*, pp.2179-2184, 2000.

[11] I.Kao and F.Yang, "Stiffness and Contact Mechanics for Soft Fingers in Grasping and Manipulation," *IEEE Trans. Robot. Automat.*, vol.20, no.1, pp.132-135, 2004.

[12] J.L.Johnson, "Contact Mechanics," Cambridge University Press, Chapter 4, 1985.
[13] Y.Tatara, "On Compression of Rubber Elastic Sphere Over a Large Range of Displacements-Part I:Theoretical Study," *ASME J. Engineering Materials and Technology*, vol.113, pp.285-291, 1991.
[14] T.Inoue and S.Hirai, "Study on Hemispherical Soft-Fingered Handling for Fine Manipulation by Minimum D.O.F. Robotic Hand," in *Proc. IEEE Int. Conf. Robot. Autom.*, pp.2454-2459, 2006.

PLACE PHOTO HERE

Takahiro Inoue was born in Osaka, Japan, on February 14, 1973. He received the B.S. degree in Mechanical Engineering at Osaka Institute of Technology, Japan, in 2002, at which time he was presented with the Hatakeyama Award from JSME. He then received the M.S. degree in 2004 and is currently working toward the Ph.D. degree in both Information Science and Engineering at Ritsumeikan University, Japan, where he is now a COE Research Fellow funded by Japan Society of the Promotion of Science (JSPS).

He received the finalist of Best Manipulation Paper Award of IEEE Int. Conf. on Robotics and Automation at 2005 and 2006. His research interests include soft-fingered manipulation, soft object modeling, and MEMS technology. He is a student member of IEEE, RSJ, SICE, and JSME.

PLACE PHOTO HERE

Shinichi Hirai was born in Fuji, Japan, in 1963. He received the B.S., M.S., and Doctoral degrees in applied mathematics and physics from Kyoto University in 1985, 1987, and 1991, respectively. He is currently a Professor in the Department of Robotics at Ritsumeikan University. He was a Visiting Researcher at Massachusetts Institute of Technology in 1989 and was an Assistant Professor at Osaka University from 1990 to 1996. His current research interests are modeling and control of deformable structures, realtime computer vision, and soft-fingered manipulation. He received SICE (Society of Instrument and Control Engineers) Best Paper Award at 1990, JSME (Japan Society of Mechanical Engineers) Robotics and Mechatronics Div. Achievement Awards at 1996, the finalist of Automation Best Paper Award at 2001 IEEE Int. Conf. on Robotics and Automation, and the finalist of Manipulation Best Paper Award at 2005 and 2006 IEEE Int. Conf. on Robotics and Automation. He is a member of IEEE, RSJ, JSME, and SICE.